Tectonophysics 692 (2016) 265–277

Contents lists available at ScienceDirect

Tectonophysics

journal homepage: www.elsevier.com/locate/tecto

Transient deformation induced by groundwater change in Taipei metropolitan area revealed by high resolution X-band SAR interferometry

Hsin Tung [a], Horng-Yue Chen [b], Jyr-Ching Hu [a,*], Kuo-En Ching [c], Hongey Chen [a], Kuo-Hsin Yang [d]

[a] Department of Geosciences, National Taiwan University, No. 1, Sec. 4, Roosevelt Road, Taipei 10671, Taiwan
[b] Institute of Earth Sciences, Academia Sinica, 128 Academia Road, Section 2, Nankang, Taipei 11529, Taiwan
[c] Department of Geomatics, National Cheng Kung University, No. 1, University Road, Tainan City 701, Taiwan
[d] Department of Civil and Construction Engineering, National Taiwan University of Science and Technology, Taipei 10607, Taiwan

ARTICLE INFO

Article history:
Received 8 March 2015
Received in revised form 21 January 2016
Accepted 21 March 2016
Available online 29 March 2016

Keywords:
INSAR
Piezometry
Land subsidence
GPS

ABSTRACT

We present precise deformation velocity maps for the two year period from September 2011 to July 2013 of the northern Taiwan area, Taipei, by using persistent scatterer interferometry (PSI) technique for processing 18 high resolution X-band synthetic aperture radar (SAR) images archived from COSMO-SkyMed (CSK) constellation. According to the result, the highest subsidence rates are found in Luzou and Wuku area in which the rate is about 15 mm/yr and 10 mm/yr respectively in the whole dataset. However, dramatic change from serve subsidence to uplift in surface deformation was revealed in the Taipei Basin in two different time spans: 2011/09–2012/09 and 2012/09–2013/07. This result shows good agreement with robust continuous GPS measurement and precise leveling survey data across the central Taipei Basin. Moreover, it also represents high correlation with groundwater table. From 8 well data in the Taipei basin, the storativity is roughly constant across most of the aquifer with values between 0.5×10^{-4} and 1.6×10^{-3} in Jingmei Formation and 0.8×10^{-4} and 1.4×10^{-3} in Wuku Formation. This high correlation indicated that one meter groundwater level change could induce about 9 and 16 mm surface deformation change in Luzou and Wuku area respectively, which is about eight times faster the long-term tectonic deformation rate in this area. Thus, to access the activity of the Shanchiao Fault, it is important to discriminate tectonic movement from anthropogenic or seasonal effect in the Taipei Basin to better understand the geohazards and mitigation in the Taipei metropolitan area.

1. Introduction

Severe land subsidence has been studied in urban areas worldwide with consequences of the exhaustion of groundwater resources, increase of risks of in flooding and damage of infrastructures and buildings (e.g. Abidin et al., 2001; Teatini et al., 2005; Konikow and Kendy, 2005; Galloway and Hoffmann, 2007; Phien-wej et al., 2006; Hu et al., 2006; Chen et al., 2007; Lai et al., 2010; Chaussard et al., 2013, 2014). Based on the recent studies, over pumping of ground water could lead to rapid subsidence at rates of up to several tens of centimeters per year. (e.g., Bell et al., 2008; Tung and Hu, 2012; Chaussard et al., 2013, 2014). Pumping-induced subsidence is primarily due to irreversible compaction of aquitard material composed of fine-grained silt and clay layers, and from minor amount of presumably elastic compaction from compression of coarse-grained conglomerate and sand deposits in aquifers (Holzer, 1984; Wilson and Gorelick, 1996; Waltham, 2002). Consequently, the elevation changes are proportional to variations of the thickness of the compaction layer and hydraulic head (Wilson and Gorelick, 1996). Thus ground elevation change due to pumping generally reflects the response to piezometric level drop. On the other hand, small amounts of land uplift might occur due to the groundwater recovery from aquifer recharged after long-term massive groundwater extraction (Amelung et al., 1999; Lu and Danskin, 2001; Schmidt and Bürgmann, 2003; Chen et al., 2007). This effect is considered to be originating from relaxation of elastically compressed aquifer materials when pore-pressure regained (Allen and Mayuga, 1969; Waltham, 2002).

In Taiwan, groundwater has been abundantly used as an alternative to surface water in urban area and in the southwestern coastal region where the deficiency of surface water resources was severe due to the high water demand from aquacultural and industrial utilization in Taiwan. Anthropogenic ground subsidence induced by heavy withdrawal of groundwater has been monitored by precise leveling, GPS measurement and SAR interferometry (e.g., Hou et al., 2005; Hwang et al., 2008; Hsieh et al., 2011; Hung et al., 2010, 2011; Wang et al.,

* Corresponding author.
E-mail addresses: cuzn0517@gmail.com (H. Tung), chenhy@earth.sinica.edu.tw (H.-Y. Chen), jchu@ntu.edu.tw (J.-C. Hu), jingkuen@mail.ncku.edu.tw (K.-E. Ching), hchen@ntu.edu.tw (H. Chen), khy@mail.ntust.edu.tw (K.-H. Yang).

http://dx.doi.org/10.1016/j.tecto.2016.03.030
0040-1951/

2011; Tung and Hu, 2012). In addition, based on the fifteen years of PSInSAR-derived surface deformation in western Taiwan, Huang et al. (2016) suggested that the seasonal displacement is mainly associated with groundwater recharge and withdrawal.

Taipei City is the political and economic centre of Taiwan (Fig. 1a) with a dense population of about 3 million. Massive groundwater pumping resulted in both dry-ups of wells and severe land subsidence during 1955–1970 (Wu, 1987). Groundwater table was gradually recovered and became approximately stable since late 1990s after a stop on the use of groundwater during the early 1970s (Chia et al., 1999). According to recent study, Chen et al. (2007) proposed that the overall subsidence rate due to the summation of shallow soil compaction, deformation within aquifer, and tectonic subsidence within the Taipei Basin gradually decreased since 1975, and around 1989 the basin switched to slight uplift throughout a large part of the basin based on the contour maps created from the leveling data of 406 benchmarks. The shallow components of soil compaction were estimated in a range of 2–3.5 mm/yr in Wuku and central Taipei Basin. Meanwhile the deep component from tectonic load was estimated in a range of 0.9–1.8 mm/yr. Furthermore, while severe anthropogenic land subsidence has been stopped in the Taipei metropolitan area, concerns on potential earthquakes associated with possible reactivation of the active Shanchiao Fault (Fig. 1b) is a crucial topic for assessment of geohazards in Taipei metropolitan area (Teng et al., 2001; Huang et al., 2007; Shyu et al., 2005).

The previous GPS network from campaign-mode survey, the GPS velocity in the Taipei Basin was insignificant in comparison with western Foothill in south-central Taiwan (Yu et al., 1997). Based on these data, Hu et al. (2002) calculate the strain rate in Taipei area, where the subnetworks NT1–NT4 have shown small extension rates (0.07–0.15 μstrain/year) and small contraction rates (0.03–0.09 μstrain/year). In addition, the extension deformations in these networks mostly trend east–west to east-northeast (Hu et al., 2002). For the period 1995–2005, 125 campaign-surveyed GPS sites in northern Taiwan had been calculated for accommodation in deformation from collision to subduction (Rau et al., 2008). These results suggested that across Chinshan–Shanchiao Faults, GPS vectors showed a slight clockwise rotation of 30° (from 303° to 332°) with magnitudes of 1.3–4.3 mm/yr from west to east.

Radar interferometry technique has proven to be capable of measuring surface displacement at fine space resolution of tens of meters over wide coverage (e.g., Massonnet and Feigl, 1998; Bürgmann et al., 2000; Pritchard and Simons, 2002; Wright, 2002). However, temporal and spatial decorrelations of radar signal have prevented this technique from more frequent utilization. Besides, the accuracy of InSAR measurements may be largely reduced by atmospheric phase artifacts that are difficult to be removed from SAR interferograms (e.g., Buckley et al., 2003; Ding et al., 2004). Consequently persistent scatterer (PS) technique has been proposed to improve the applicability of radar interferometry when applied to detect long-term ground deformation with tracking the signals of discrete point-wise targets (Ferretti et al., 2000, 2001; Berardino et al., 2002; Mora et al., 2003; Hooper et al., 2004; Kampes and Hanssen, 2004; Liu et al., 2008). According to previous studies, a surface deformation map of northern Taiwan using SAR interferometry technique from 1993 to 2005 has been shown by Chang et al. (2010). They suggested that the significant subsidence occurred at the border of the Taipei Basin and a relatively slight uplift rebound in the central basin, and displacements along the Shanchiao, Chinshan, and Kanchiao Faults are large enough to be observed. However, part of surface deformation from SAR interferometry should be related to the groundwater recharge and withdrawal (Huang et al., 2016). In this paper, we use the high resolution X-band SAR images from COSMO-SkyMed (CSK) constellation with the constraints of leveling and

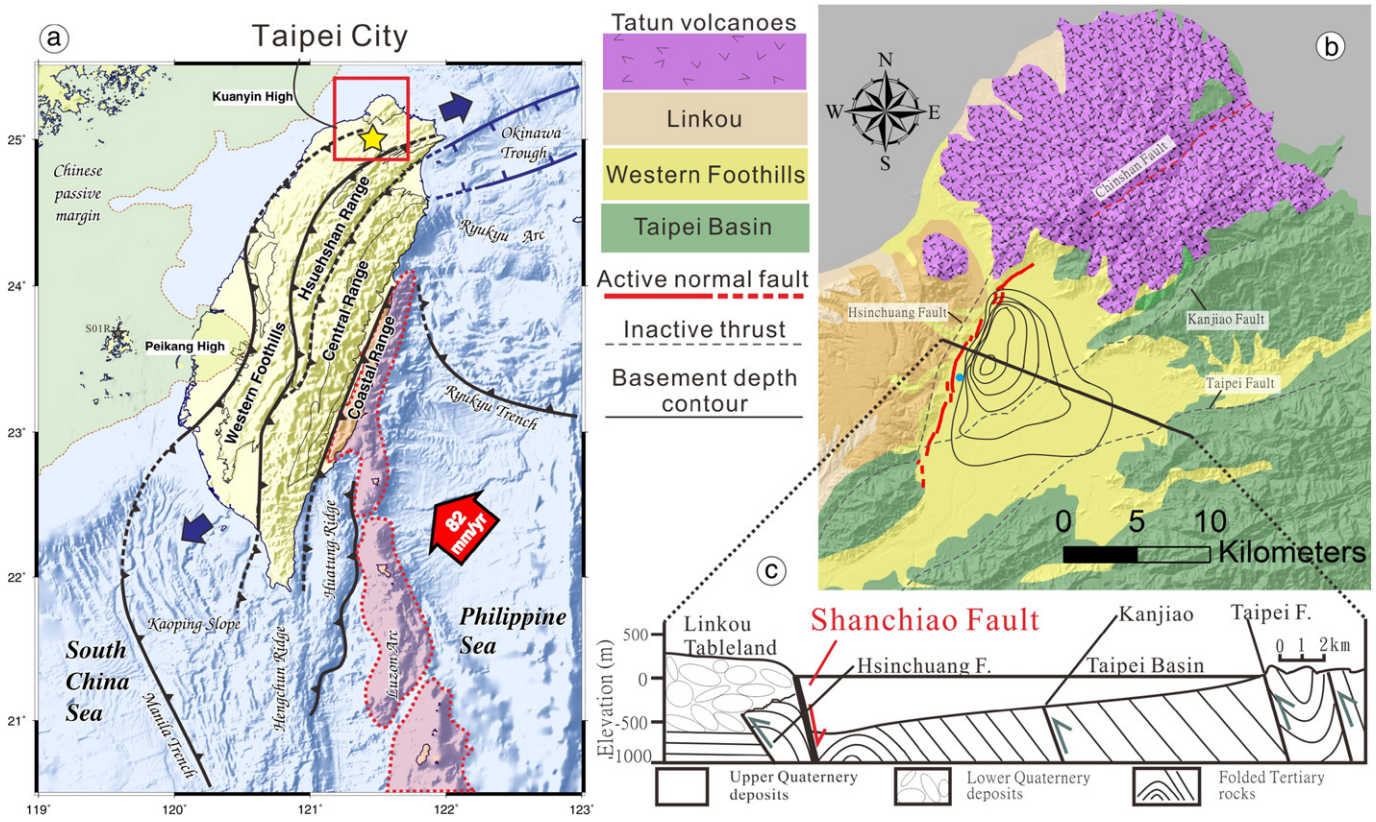

Fig. 1. (a) Tectonic framework of Taiwan. (b) Geological domains of Taipei region. The thin black lines within Taipei Basin indicate the basement depth contour of 100 m interval. (c) Geological cross section of the Taipei Basin (modified from Chen et al., 2007). Blue dot is the location for stratigraphic architecture of late Quaternary deposits in Fig. 2.

continuous GPS data to monitor surface deformation in the Taipei area and characterize the transient surface deformation due to the groundwater recharge and withdrawal.

2. Geological setting and data

2.1. Geological and hydrological background

From the tectonic viewpoint, Taiwan Island is situated at the plate suture of Eurasian and Philippine Sea plate since 5 Ma (e.g., Suppe, 1981; Teng, 1990). According to GPS results, the convergence rate is about 82 mm/yr in the NW direction (Yu et al., 1997; Lin et al., 2010). At present, the collision process is manifested in southern and central Taiwan as demonstrated by the intense crustal shortening and frequent seismicity. In contrast, north-eastern Taiwan underwent post-collisional processes and has been considered to be incorporated in the opening of the southern Ryukyu back-arc system (Teng et al., 2000). Opening of Okinawa Trough and the retreat of Ryukyu trench together with the ongoing collision process in north-western Taiwan results in transtensional and extensional regimes (Hu et al., 1996, 2001, 2002), as revealed by the presence of Quaternary extensional structures (Lee and Wang, 1988; Lu et al., 1995), extensional earthquake focal mechanisms (Kao et al., 1998) and GPS measurement (Yu et al., 1999; Hu et al., 2002; Rau et al., 2008). The Taipei Basin is located at the northern part of Taiwan, surrounded by Tatun Volcano group to the north, the Linku Tableland to the west, and the northwest hills of western Foothills and Hsüehshan Range to the southeast (Fig. 1a and b). The active Shanchiao Fault bounding the western edge of the Taipei Basin is an east-dipping normal fault with a dip angle of about 60°. The average late-Quaternary long-term tectonic subsidence rate was estimated by stratigraphic offset across the fault to be 1.75 mm/yr since 0.4 Ma. This active fault is, and should have an influence on the elevation change in the western Taipei Basin (Chen et al., 2007).

The seismicity in the Taipei Basin is lower than the other area of northern Taiwan (e.g. Kim et al., 2005; Wang et al., 2006; Konstantinou et al., 2007). In addition, with the lock of cluster seismicity and seismic profile in the Taipei Basin, it is difficult to correlate the seismicity with recognized faults. At least there Holocene paleoseismic events with a slip of 1–3 m were proposed at ~8500, ~9200, and ~11,100 years B.P. from analysis of basin sediments retrieved from shallow boreholes in the Taipei Basin (Huang et al., 2007). The dense broadband seismic array was deployed to monitor seismicity in the Taipei Basin since June 2004 (Chen et al., 2010b). During the period of observation, three felt earthquakes (M_L = 3.8, 3.2, and 3.7) of normal faulting happened near the eastern part of the basin. The focal depth of ~9 km was proposed to be related to a blind fault under the Taipei Basin (Chen et al., 2010b) and was triggered by the loading of famous Taipei 101 building (Lin, 2005). Recently Chen et al. (2014) interpreted that three felt earthquakes are located in the junction of the shallow border of the lower fault ramp and inverted thrust detachment of active Shanchiao Fault.

The Taipei Basin has been a dammed lake associated with the last eruption of Tatun volcanism which blocked the effluence of the Tanshui River at about 0.2 Ma (Song et al., 2000). After that, global climate change brought marine transgression and made this place to an estuarine deposition at around 6 Ka. According to the deep drill data, the triangular-shaped Taipei Basin is considered as a half-graben filled with deformed Tertiary strata and filled with upper Pleistocene and Holocene sediment since about 0.4 Ma (Wei et al., 1998; Teng et al., 2001), and the deepest basement is close to the active Shanchiao Fault with depth more than 670 m (Fig. 1b). The stratigraphic section cutting through the central Taipei Basin shows that the basin sediment, dominated by gravel, sand, mud and their interbred is formed by late-Quaternary fluvial formation laying on the top of the Miocene sedimentary bedrock. These unconsolidated deposits can be divided into four lithostratigraphic units with two basin-wide marker beds, Jingmei gravel and Banqiao lake mud (Fig. 2). From top to bottom: (1) the Sungshan

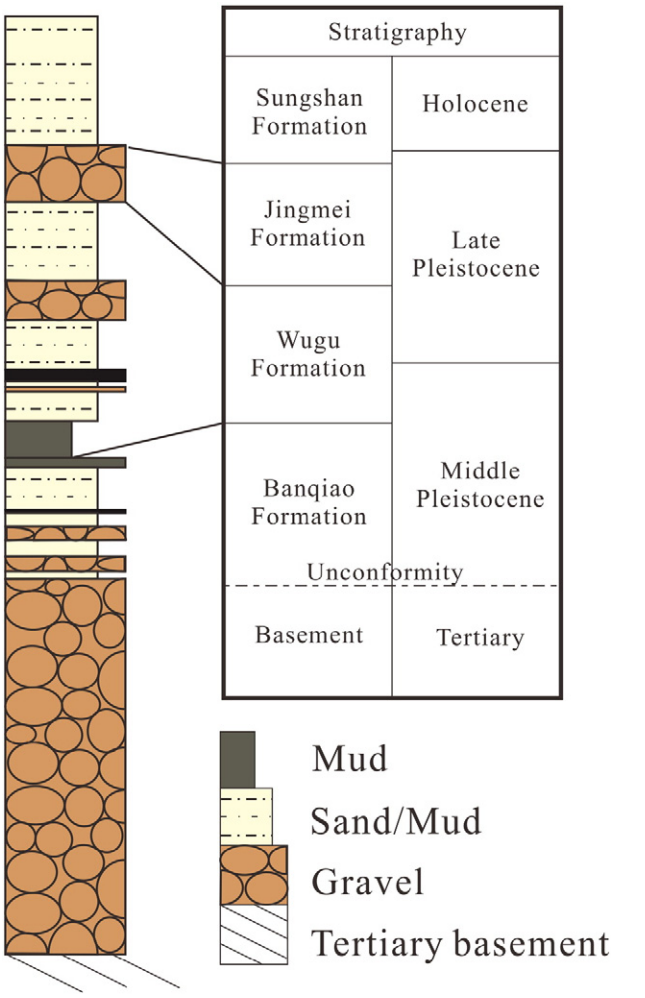

Fig. 2. Stratigraphic architecture of late Quaternary deposits within Taipei Basin (modified from Teng et al., 1999). Location see Fig. 1b (blue dot).

formation, composed of estuary interbedded with sand and mud deposits, is an unconfined aquifer with three aquifers and three aquitards; (2) the Jingmei formation, formed by lateritic alluvial-fan conglomerates is the main aquifer of the Taipei Basin with hydraulic diffusivity around 0.12 to 0.18 m^2/s and storage coefficient ranging from 0.001 to 0.004 (Chia et al., 1999); (3) the Wuku formation, consisted of fluvial sand and conglomerates with minor mud and lateritic conglomerates; (4) the Banqiao formation, comprised of fluvial sand, mud and conglomerates, with minor pyroclastic debris and thick mud in the upper section (Teng et al., 1999).

Since the 1950s, serious land subsidence occurred from the extensive pumping from the aquifer in the Taipei Basin due to the demand of accumulated populations. The groundwater level has declined approximately 50 m before 1976 and followed by a rapid recovery starting from the late 1970s. Following up, according to the recent study analyzed from leveling data, Chen et al. (2007) proposed that the post-pumping phenomena indicated the subsidence rate for the Taipei Basin as a whole generally decreased trend from 40–70 mm/yr to 0–30 mm/yr during 1975 to 1989, and then the elevation change of the basin gradually switched to a slight uplift from 10 to 15 mm/yr in central Taipei and Banqiao since about 1989.

2.2. Continuous GPS and precise leveling data

Totally 14 continuous GPS station are calculated for velocity field in study area with respect to continuous WUKU GPS station, which is

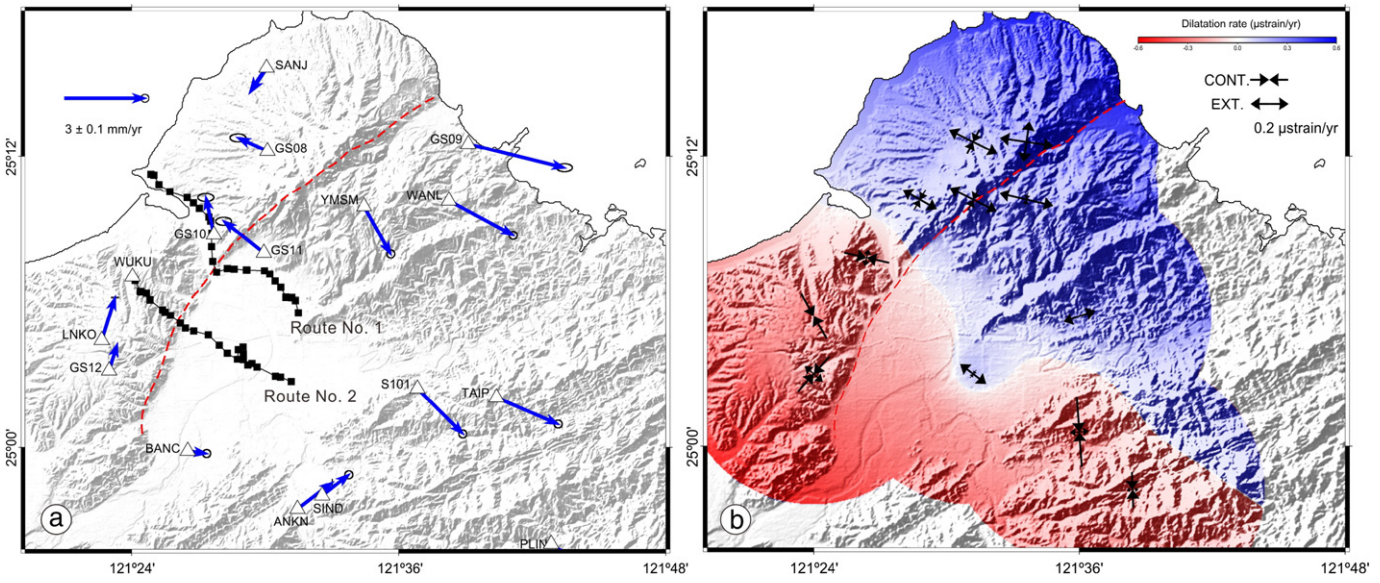

Fig. 3. (a) Continuous GPS velocity field with respect to WUKU located in stable Linko tableland. Red line represents the Shanchiao and Chinshan Faults. Black squares represent the benchmarks of two precise leveling routes. (b) Horizontal principal strain rate and dilatation rate based on continuous GPS data.

located at relative stable Linko tableland on the western Taipei Basin from 2006 to 2015. The GPS velocity ranges from 0.7 mm/yr to 3.7 mm/yr (Fig. 3). From viewpoint of deformation rate, two deformation regimes are observed; a contractional regime in southern part of the Shanchiao Fault and an extensional regime in northern part of the study area. The maximum NW–SE contractional principal strain rate that is about

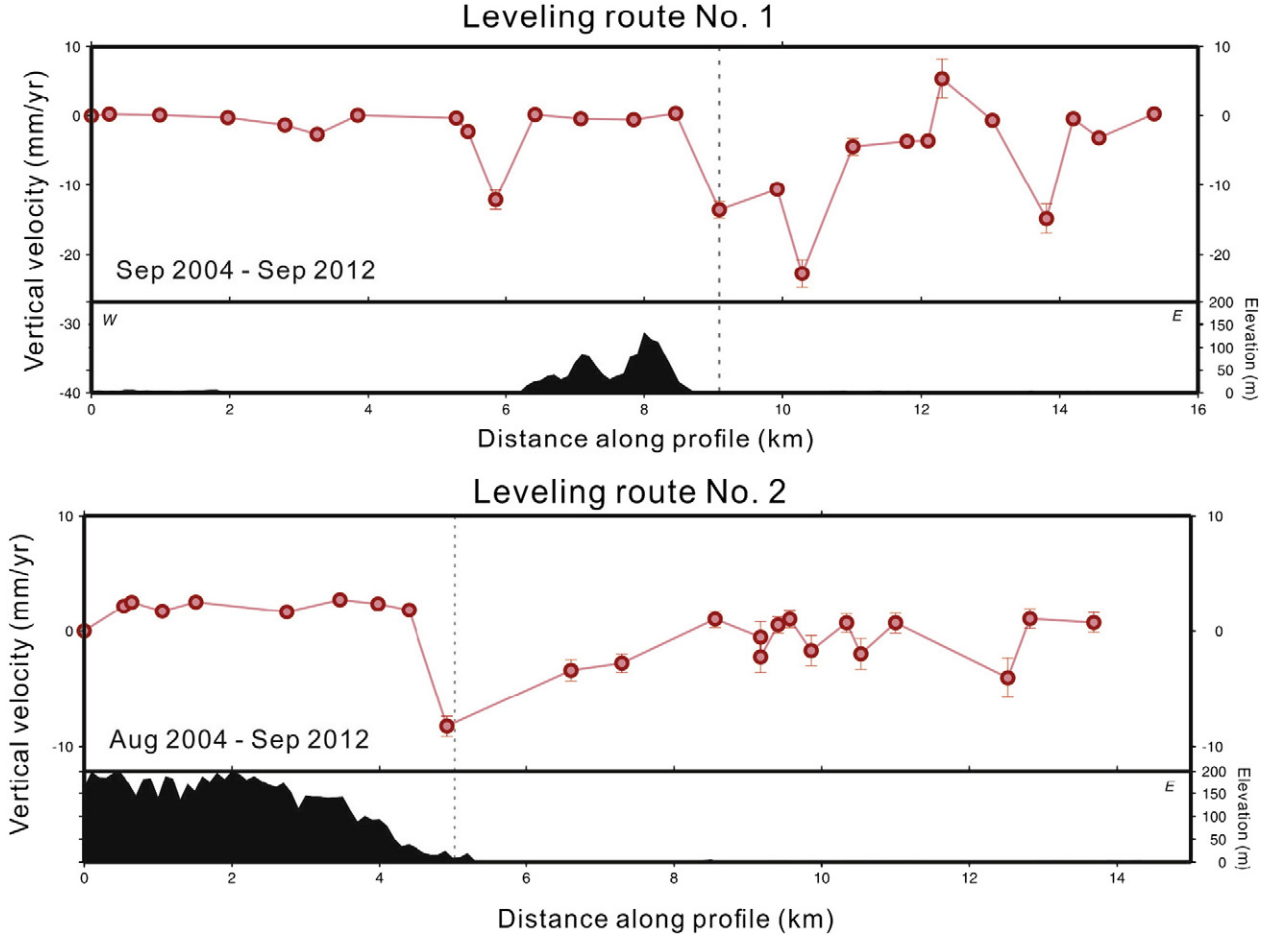

Fig. 4. Vertical velocity profile of two precise leveling routes across the Shanchiao Fault in north (No. 1) and central Taipei area (No. 2). Location of leveling routes is shown in Fig. 3. Red dots represent the vertical velocity and gray dotted line represent the location of the Shanchiao Fault.

0.37 μstrian/yr occurred in the footwall of the Shanchaio fault. The WNW–ESE extensional principal strain rate of about 0.28 μstrian/yr occurred near the Tatung Volcano.

Two precise leveling routes across the Shanchiao Fault are deployed by Central Geological Survey for monitoring the ground deformation. The westernmost benchmark of leveling route is used for reference point (Fig. 4). In general, both leveling routes show no significant elevation change in the footwall of the Shanchiao Fault, except one benchmark on leveling route No. 1 showing a local subsidence rate of 10 mm/yr. Near the Shanchiao Fault, two leveling routes show similar trends of increasing of land subsidence rate. In addition, the subsidence rate mostly decreases westward to central Taipei Basin. The maximum land subsidence rate is about 20 mm/yr and 10 mm/yr observed in routes No. 1 and No. 2, respectively from September 2004 to September 2012.

2.3. Methodology and SAR data acquisition

Interferometric synthetic aperture radar (InSAR) technique has been applied widely in surface displacement measurements since the first coseismic displacement pattern of Landers earthquake published on the cover of Nature (Massonnet et al., 1993). Its advantages of fast and wide cover observations provide an effective tool in geodetic survey (e.g., Massonnet and Feigl, 1998; Bürgmann et al., 2000). An advanced InSAR technique that traces movements of pixels in a bunch of radar images called persistent scatterer SAR interferometry (PSInSAR) technique has been proposed to improve the applicability of image analysis. This technique overcomes the limitations of temporal and atmospheric bias in conventional InSAR technique by computing only on sparsely distributed persistent scatterers (PSs). Through this process, the signals which cannot be obtained from conventional InSAR technique will be retrieved and the accuracy of displacement rate measurements increases from cm to mm scale.

The PSInSAR technique is an advanced technique in comparison with conventional InSAR technique, which addresses the problems of decorrelation for generating a time series of phase changes without atmospheric and DEM residuals effects by computing only on sparsely distributed PSs which are pixels coherent over long time series. This technique has been developed in the late 1990s by A. Ferretti, F. Rocca, and C. Prati of the Technical University of Milan (POLIMI). The first algorithm to find out the PS pixels was brought (Ferretti et al., 2000), and trademarked it as the "Permanent Scatterer technique". After that, similar processing algorithms have since been developed by Crosetto et al. (2003), and Mora et al. (2003). Besides, the Small Baseline subset technique developed by Berardino et al. (2002) and StaMPS (Stanford Method for Persistent Scatterers) developed by Hooper et al. (2004) are also the same idea of the PSInSAR technique with different names. The application of PSInSAR technique in the study of active faults and land subsidence in Taiwan has proven to be capable of measuring ground deformation at fine space resolution over wide coverage (Chang et al., 2010; Peyret et al., 2011; Champenois et al., 2012; Tung and Hu, 2012; Wu et al., 2013)

The stripmap mode of CSK SAR images provides spatial resolution of 3 m × 3 m, which is one order of magnitude better than the previous available satellite SAR data. The higher resolution leads to an increase of the density of the measurable targets relatively to those retrieved from medium resolution datasets (C- and L-band). On the other hand, the sensitivity of displacements is increased with shorter wavelengths (~3 cm), which enhance the capability of detecting very slow displacements rates. Furthermore, the more frequent revisit of the same Area of Interest (AOI) of the present X-band missions provides massive datasets to avoid the baseline limitation and temporal decorrelation, which improve the temporal resolution of deformation in time series.

Totally 18 ascending COSMO_Skymed constellation (Constellation of Small Satellites for Mediterranean basin observation) images were used for processing interferograms from September 2011 to July 2013. Most of the interferograms have an absolute normal baselines smaller than 500 m (Fig. 5). Raw radar images were focused using ROI_PAC software developed by the JPL/Caltech; Interferograms were formed using Doris software (Kampes and Usai, 1999). The PSI was processed with StaMPS/MTI (Stanford Method for Persistent Scatterers/Multi Temporal InSAR). The topography phase component was removed by using SRTM DEM (3 arcsec in resolution) during interferogram processing. The details of images' information are shown in Fig. 5.

3. Result and analysis

In this study, 18 radar images were used to form 17 PSI interferograms. The Taipei Basin is a metropolis with dense artificial structure, giving a good condition for processing PSs. Within the 750 km^2 of the study area, roughly 1035,000 stable targets were available (Fig. 6). The density is 1380 points/km^2, which is almost 1000 times denser than other geodesy survey like leveling and GPS.

Continuous GPS data calculated by using GIPSY/OASIS software to estimate the precise coordinates and 3D-velocities and then convert the direction of motion to radar LOS (line-of-sight) component with incident angle of 23° (Fig. 6). In order to understand the deformation pattern in and around the Taipei Basin, the null-reference PS velocity is set in the vicinity of the continuous WUKU GPS station, which is located at relative stable Linko tableland on the western Taipei Basin illustrated in Fig. 6. After referencing to a relative stable WUKU station, the contribution of deformation in the horizontal direction is reduced. Then the 3D velocity filed of the six continuous GPS stations (LNKO, BANC, GS10, GS11, GS12 and S101) is projected to LOS to compare with the average LOS rate from the PSInSAR. The color shown in triangle is the LOS rate projected from GPS velocity and that in circle is the LOS rate from PSInSAR. The comparison of these two LOS rates are in good agreement.

The most significant signal is slight subsidence on the Luzhou and Wuku area with LOS deformation rate away from satellite 10 mm/yr and 5 mm/yr respectively. The subsidence areas are located close to the Shanchiao Fault. Another conspicuous pattern can be observed on the Beitou spring area, the LOS velocity rate of 10–15 mm/yr, indicating an active uplift occurred in this area. Unfortunately, no geodetic measurements and continuous GPS station were deployed in this area, thus we can't characterize the implication of this uplift so far. Only two continuous GPS stations (GS10 and GS11) showing inconsistent LOS deformation rate with that from PSInSAR, this inconsistence might be attributed by phase unwrapping error due to cross the river. Most of the PS points show consistent deformation rate with continuous

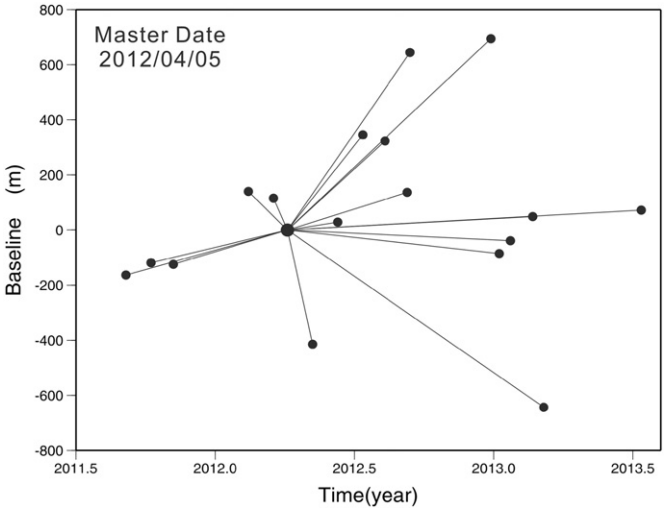

Fig. 5. Radar images and baseline information used in this study. Vertical axes are perpendicular baselines of image pairs relative to the master image on 5 April 2012; horizontal axes are acquisition dates of radar images.

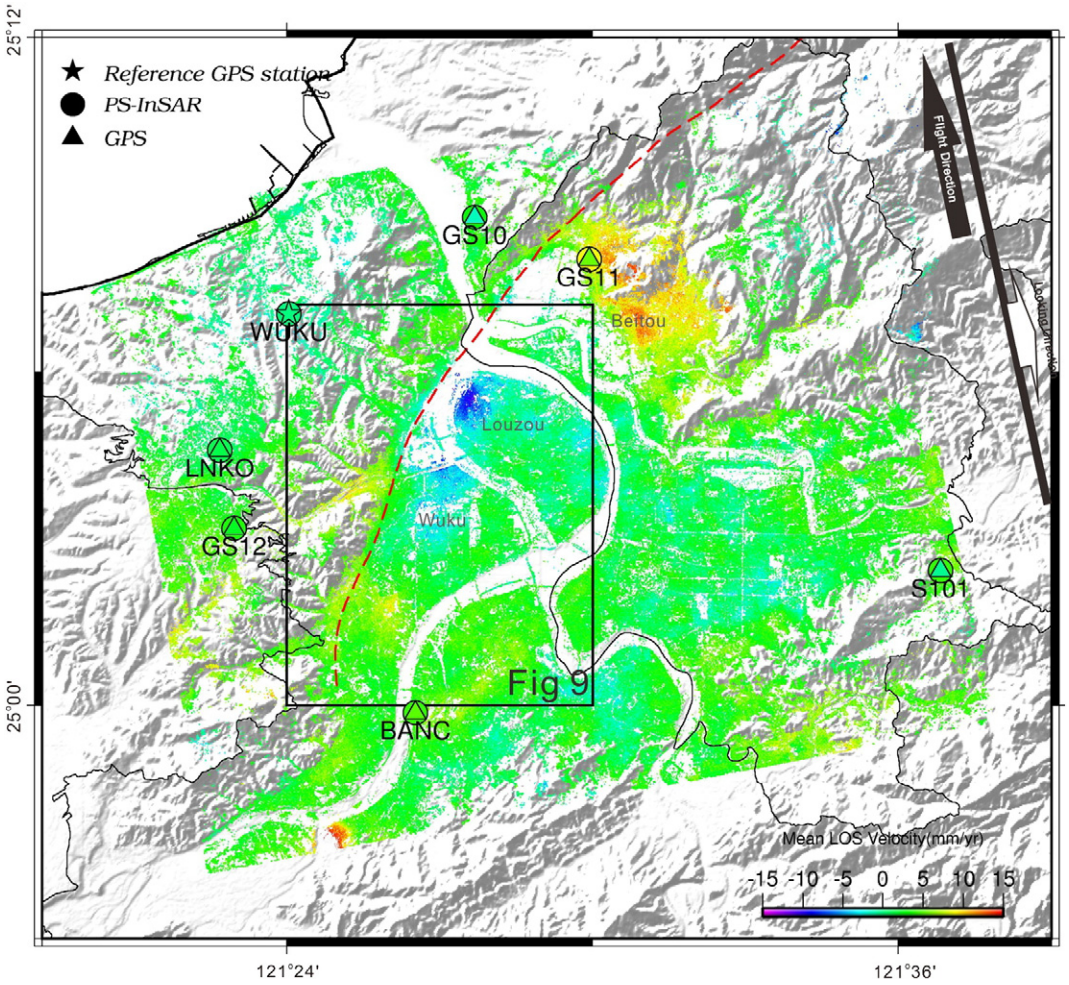

Fig. 6. Slant range displacement rate of the processed PSs in the northern Taiwan area overlapped on the hill-shaded background. Shortening in slant range (rate in positive with warm colors) represents land uplift and elongation (rate in negative with cold colors) represents land subsidence in slant range direction. Red dashed lines mark the active Shanchiao Fault (Lin et al., 2000). Colored triangles represent transferred GPS velocity from 3D to LOS direction and colored circles represent average velocities of PS points within 100 m of the GPS station in LOS direction. Rectangle is the location of Fig. 9.

GPS stations, the velocity differences between average PSs and continuous GPS station are less than 4 mm/yr. The good agreement indicates the reliability of our PSInSAR result.

Different deformation patterns have been revealed from previous studies by using precise leveling and C-band SAR data analysis (e.g., Chen et al., 2007; Chang et al., 2010). The deformation within the Taipei Basin varied from severe subsides to light uplift during 1975 and 2003 (Chen et al., 2007). Based on the study of PSInSAR and precise leveling, relatively subsidence in the Taipei Basin were observed from 2004 to 2007 (Chang et al., 2010). It is interesting to note that the dramatic changes of surface deformation in study area are observed whenever the whole dataset was separated into two sub-datasets to fit the survey period of precise leveling from 2011/9–2012/9 and 2012/9–2013/7 (Figs. 7 and 8). LOS rate from PSInSAR demonstrates that the significant land subsidence occurred in the hanging wall of the Shanchiao Fault related to the continuous GPS station WUKU located on the footwall of the fault in the period of 2011/9–2012/9 (Fig. 7a). The relatively maximum LOS rate can be up to about 5.5 cm/yr in the Taipei Basin. A good consistence shows between LOS rates of PSInSAR and the projection of 3D components of 6 continuous GPS (Fig. 7a). Independent precise leveling carried out in the same period also the similar trends on both hanging wall and footwall of the Shanchiao Fault (Fig. 7b). The maximum subsidence rate related to WUKU station is about 3 cm/yr located on the hanging wall of the Shanchiao Fault.

Surprisingly the deformation patterns on the hanging wall of the Shanchiao Fault switch to trend of uplifting related to WUKU station in the period of 2012/9–2013/7 (Fig. 8a). The relatively maximum LOS rate can be up to about 5 cm/yr in the Taipei Basin. The comparison of LOS rates from PSInSAR and projected continuous GPS rate is in good accordance. Independent precise leveling carried out in the same period also the similar trends on both hanging wall and footwall of the Shanchiao Fault (Fig. 8b). The maximum uplift rate is about 3 cm/yr related to WUKU station. The difference of LOS rate from PSInSAR and uplift rate from precise leveling are resulted from the time period inconsistent between leveling survey (~1 year) and SAR acquisitions (~10 months). We will discuss this change of deformation pattern of two periods in Discussion.

4. Discussion

4.1. Characterizing Shanchiao Fault trace form PSInSAR velocity field

High erosion rate in Taiwan and the cover of alluvium deposits make it difficult to find the active fault trace buried under the ground. Previous study of topographic mapping from LiDAR-derived DEM and real-time kinematics GPS survey had characterized the geomorphology of Shanchiao Fault zone revealed by a series of fault-related scarps arranged in an *en échelon* array (Chen et al., 2006). However the surface

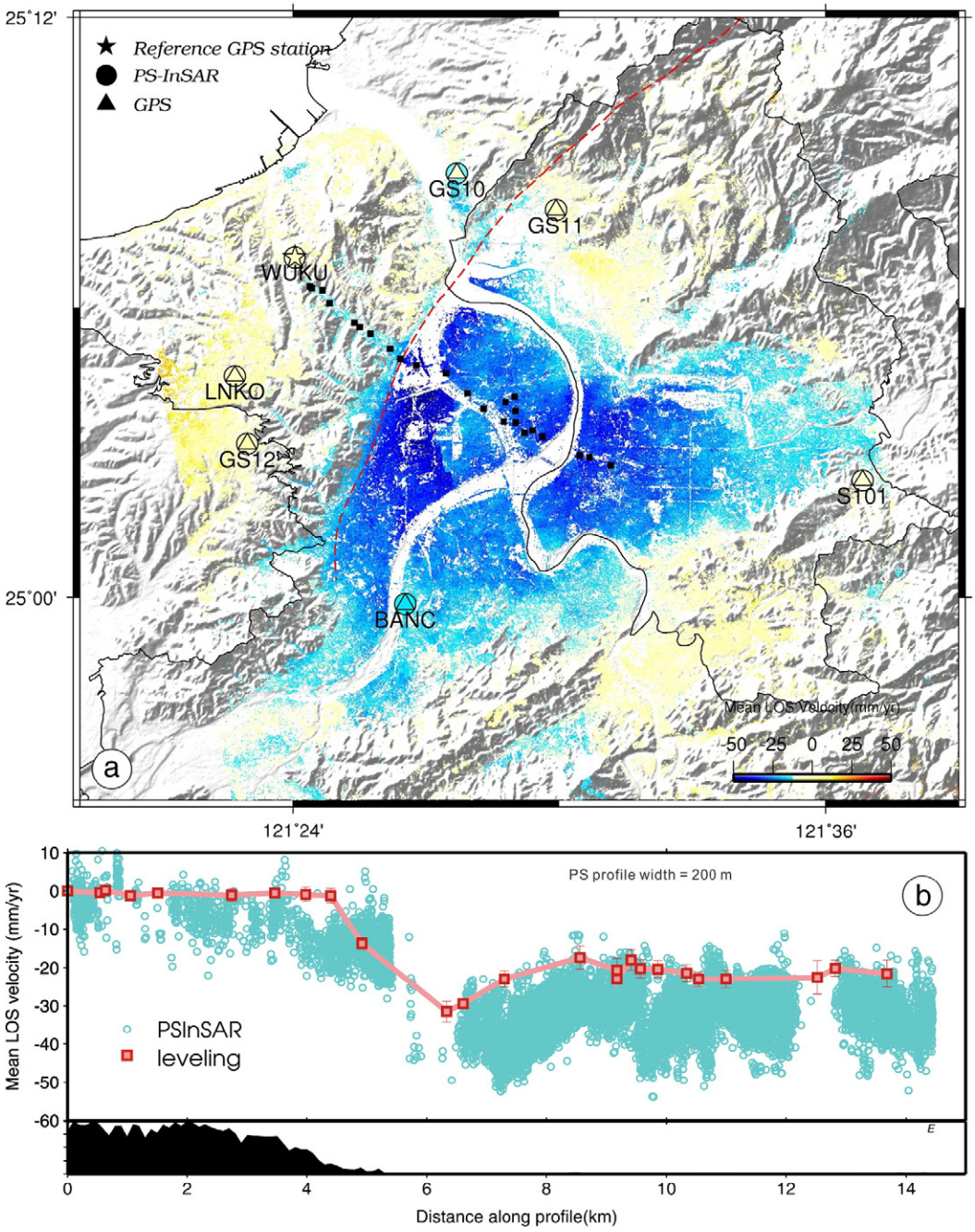

Fig. 7. (a) Slant range displacement rate of time span 2011/9–2012/9. (b) Comparison between the leveling data and PSInSAR result along the central of the Taipei Basin. Black rectangles are the locations of benchmarks in leveling route. Both PS and leveling data are relatively to the westernmost benchmark (WUKU) of the profile.

trace of the main fault seems to be completely erased by the surface force of erosion and sedimentation, only the subtle geomorphic scarps corresponding to the branch fault can be identified based on the correlation between geomorphology and subsurface geology in the Shanchiao Fault zone (Chen et al., 2010a).

In order to represent the various characters of the Shanchiao Fault, four velocity profiles sub-perpendicular to the Shanchiao fault from north to south contain PS points within 50 m have been shown in Fig. 9. The results show a significant velocity drop across the fault in profile 1; the velocity gradient is up to 5 mm/yr. In profile 2, the velocity gradient across the fault decreases to 3–4 mm/yr. Furthermore, there is no obvious velocity change in both profile 3 and profile 4. This result indicates that the Shanchiao Fault shows less activity from north to south, which might be the evidence to form the triangular-shaped half-graben observed by stratigraphy from deep drill data.

The LOS rate from the whole two years dataset of PSInSAR is superimposed on the LiDAR-derived DEM to try mapping the trace of the Shanchiao Fault in Wuku area (Fig. 10, left panel). The black dashed line is the surface trace of the Shanchiao Fault from 1:25,000-scale active fault map published by Central Geological Survey, MOEA (Lin et al., 2000); green line is morphotectonic analysis based on LiDAR-derived DEM made by Chang et al. (2014). Our PSInSAR result suggests that a localized deformation change is located between boreholes SCF-2 and WK-1 shown by navy dashed line. In addition, only slight velocity gradient changes are observed from PSInSAR profile across the Sanchiao Fault proposed by Central Geological Survey, in which Lin et al. (2010) suggested that the main Sanchiao Fault is located between boreholes SCF-1 and SCF-2. Thus surface trace of black dashed line could be the secondary fault of the Shanchiao Fault zone, which is consistent with the previous study based on the correlation between geomorphology

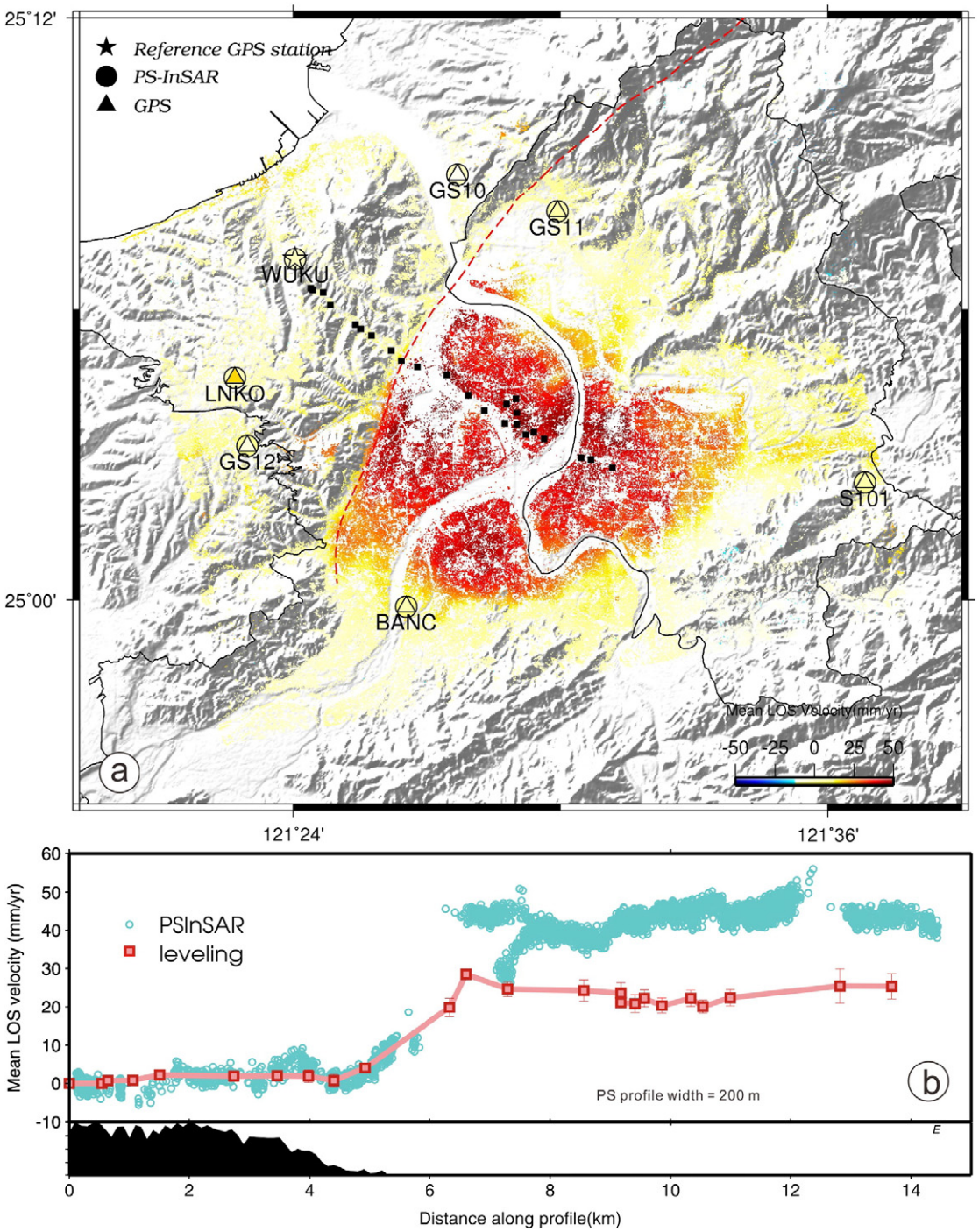

Fig. 8. (a) Slant range displacement rate of time span 2012/9–2013/7. (b) Comparison between the leveling data and PSInSAR result along the central of the Taipei Basin. Black rectangles are the locations of benchmarks in leveling route. Both PS and leveling data are relatively to the westernmost benchmark (WUKU) of the profile.

and subsurface geology of three boreholes in the Shanchiao Fault zone (Fig. 10, right upper panel, Chen et al., 2010a). By contrast, our PSInSAR result proposed that the main Shanchiao Fault is located between the boreholes SCF-2 and WK-1 (Fig. 10, right lower panel), in agreement with the study of Chen et al. (2014), Fig. 10, left panel in pink). Furthermore, our PSInSAR result can improve to map the trace of the Shanchiao Fault and rectify the limited number of borehole locations.

There is a vertical offset of Tertiary strata of more than 700 m across the north and central Shanchiao Fault (Wang et al., 1994, 1995; Teng et al., 2001, see Fig. 1b). This implies that the activity of the north-central segment of the Shanchiao Fault is higher than its southern segment. Based on average LOS rate of PSInSAR in the Taipei Basin (Fig. 6), Luzhou area shows highest gradient of LOS rate across the Shanchiao Fault, which is consistent with the maximum vertical offset in Tertiary strata in northern segment of the fault. However, spatial distribution of confined aquifers and temporal fluctuation of the groundwater are the major control factors of the ground deformation (Chen et al., 2007). Using two drilling holes data in Wuku and central Taipei, the soil compaction is in a range of 2–3.5 mm/yr and the deep tectonic load is in a range of 0.9–1.8 mm/yr. Our study indicates that one meter groundwater level change could induce about 8 and 16 mm surface deformation change in Luzou and Wuku area respectively, which is

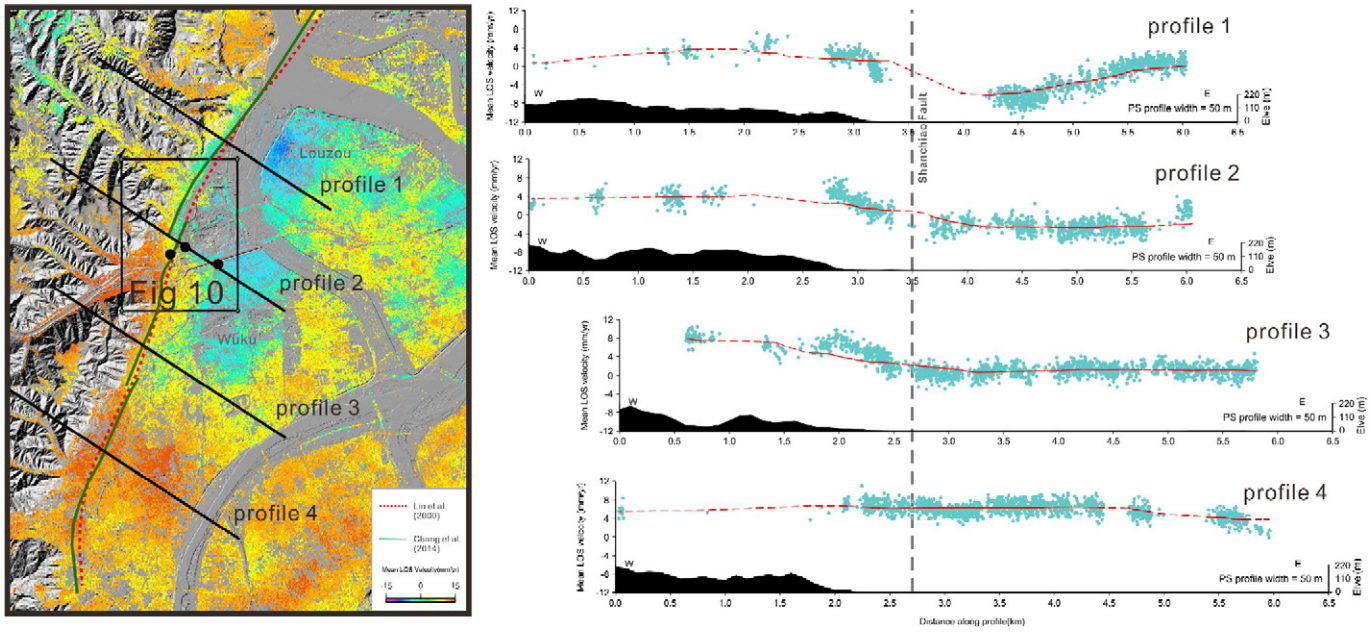

Fig. 9. Four velocity profiles of the Shanchiao Fault within the Taipei Basin. Red dash line represents 1:25,000-scale active fault map published by Central Geological Survey, MOEA; green lines represent morphotectonic analysis based on LiDAR-derived DEM. Rectangle is the location of Fig. 10. Three solid circles are boreholes sites used in Fig. 10.

about eight times faster the long-term tectonic deformation rate in this area. Consequently the aquifer deformation controls the vertical ground deformation, for instance it is difficult to characterize the along-strike deformation gradient without detailed investigation of spatial distribution and thickness of major confined aquifers in the Taipei Basin.

4.2. Extract hydraulic parameter from correlation of PSInSAR and groundwater level

Storativity (S, as well as storage coefficient) is defined as the volume of water taken into or expelled from storage per unit decline in

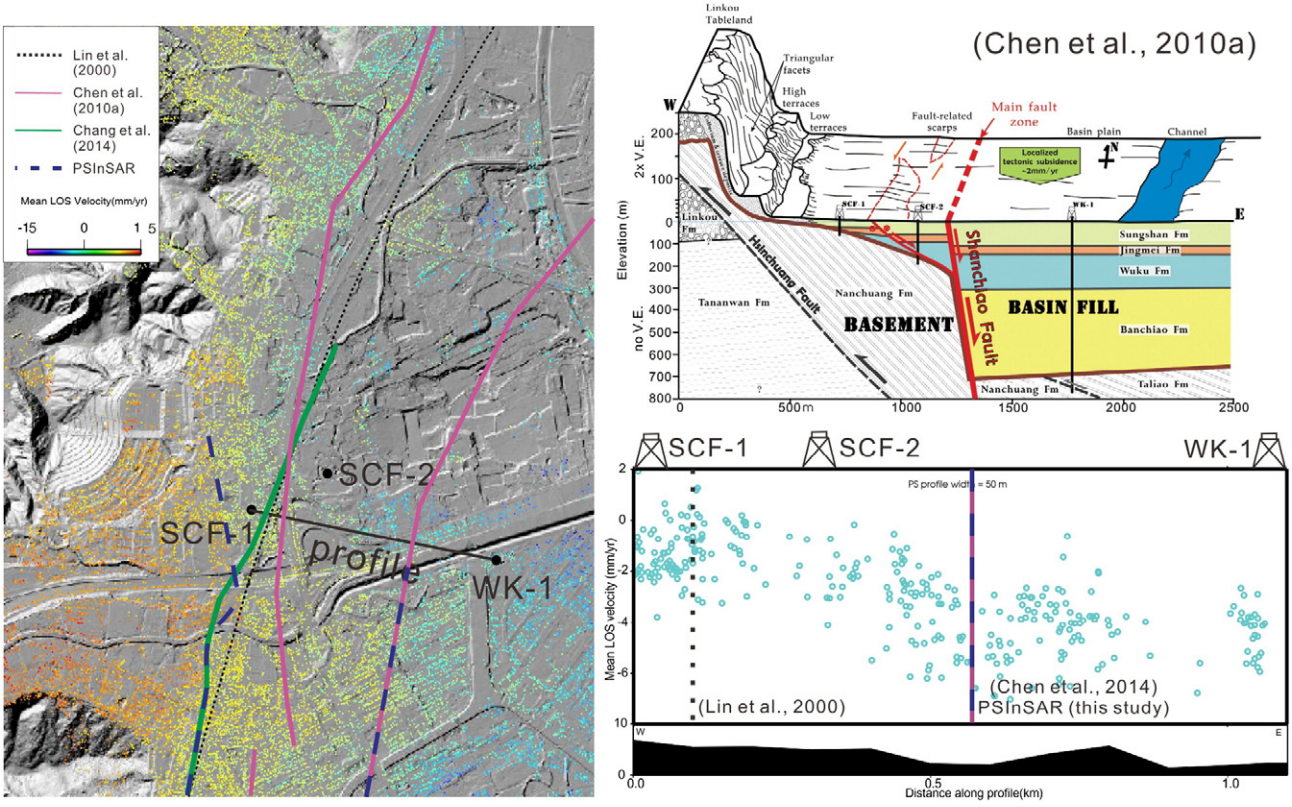

Fig. 10. Comparison of fault properties characterizing. Black dash line represents 1:25,000-scale active fault map published by Central Geological Survey, MOEA; red lines represent fault activity front decided by PSInSAR result. SCF-1 and WK-1 show the locations of two boreholes used in Chen et al. (2010a).

hydraulic head, per unit area of the aquifer. It quantifies the amount of groundwater obtained by vertical aquifer-system compaction and helps to define maximum pumping rate in the elastic range of deformation. In this paper, we use the relationship between hydraulic head changes and surface deformation (S = d/h, where d is the vertical ground displacement and h is the hydraulic head change) to characterize the storativity at the seven wells within the metropolitan Taipei City. In the period 2011/9–2012/9, the time series of PSInSAR demonstrate the decline of the LOS displacement from 10 mm to −20 mm (Fig. 11b). By contrast in the period 2012/9–2013/7, the time series of PSInSAR shows an increase of LOS displacement from −20 mm to 10 mm. Water Resources Agency of the Ministry of Economic Affairs of Taiwan installed more than 20 observation wells in the Taipei Basin to monitor the groundwater tables over the years. Here we take Wuku well as an example to demonstrate the relationship between surface deformation and groundwater level change (Fig. 11). It is worthy to know that the groundwater level shows a similar trend in the period of observation from SAR interferometry only in the Wuku(2) and Wuku(3), which are located at the Jingmei Formation and Wuku Formation, respectively (Fig. 11b). The groundwater level declines from about −6 m to −16 m in Wuku(2) and from −8 m to −18 m in Wuku(3) at the first period and recovers from −16 m to −4 m in Wuku(2) and from −18 m to −5 m in Wuku(3) at the second period. Thus we use the correlation of surface deformation from time series of PSInSAR and groundwater level to calculate the storativity in the Wuku area. The correlation between 18 points from LOS displacement and groundwater level give a storativity of 0.0016 in Jingmei Formation and 0.0014 in Wuku Formation(Fig. 11c), that is 10 m of hydraulic head change can induce about 1.4 to 1.6 cm of surface deformation. According to the stratigraphic, Wuku well is formed by sand and gravel. On the other hand, it

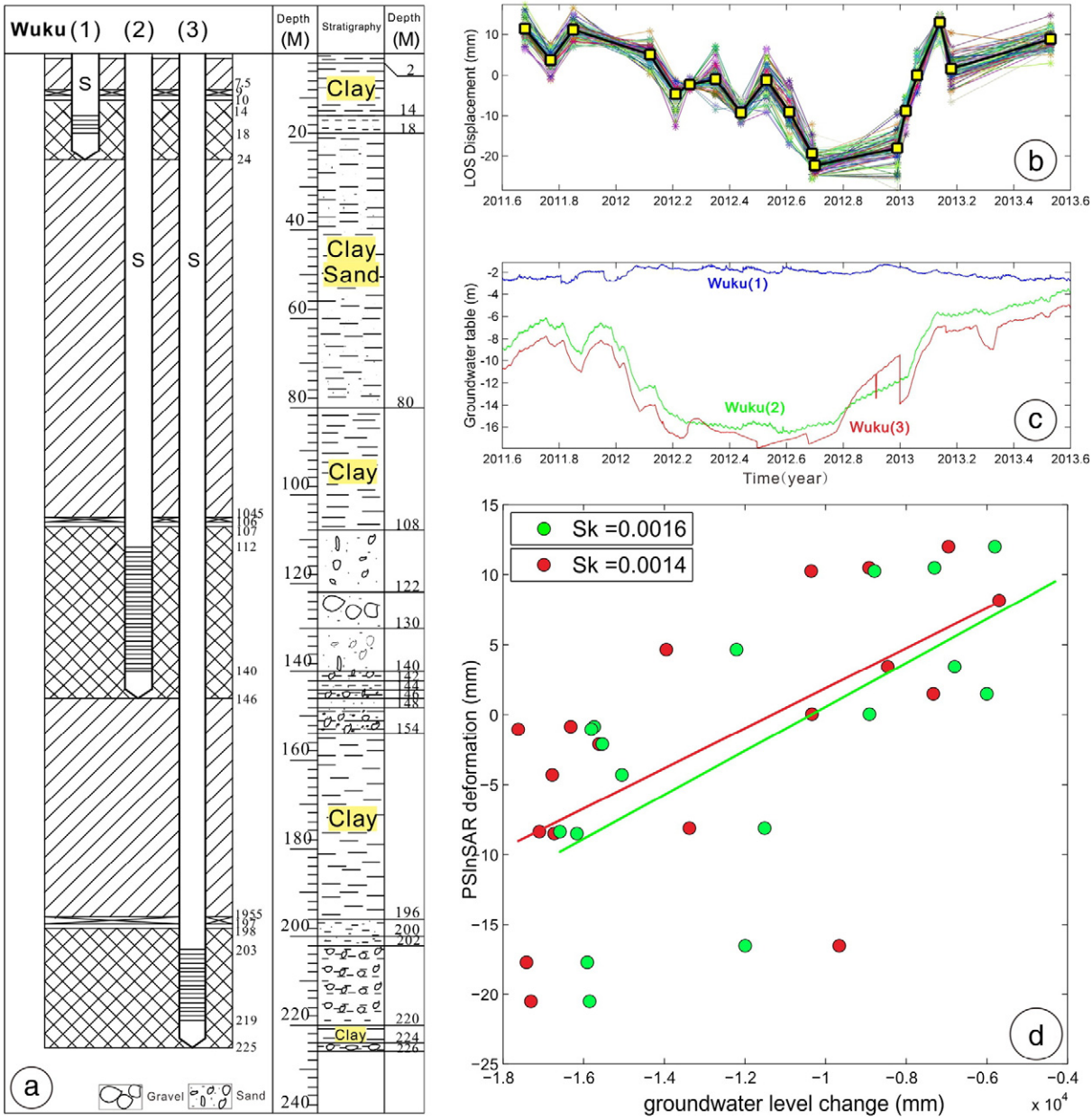

Fig. 11. (a) Stratigraphy of groundwater well Wuku. (b) Time series of average PS points value within 100 m of groundwater well Wuku. (c) Groundwater level change of groundwater well Wuku from September 2011 to July 2013. (d) Storativity calculated from surface deformation of PSInSAR and change of groundwater level. Solid line is the best fitting of linear regression; corresponds to the storativity.

Table 1
Hydrological information and storativities of 9 wells in Taipei basin.

Station name	Depth (m)	Formation	Storativity
Wuku	147.2/268.4	Jingmei/Wuku	0.0016/0.0014
Xinzhuang	107/174	Jingmei/Wuku	0.0010/0.0012
Banqiao	118.5	Jingmei	0.0005
Luzou	126.0	Jingmei	0.0009
Juangjing	79.0	Jingmei	0.0012
Erchong	96.6	Wuku	0.0010
Sanchong	107.4	Wuku	0.0013
Youth Park	85	Jingmei/Wuku	0.0008
Taida	60.0	Jingmei	−0.0006

contained thick layer clay at the depth of 18 m to 108 m and 154 m to 196 m, which might be the main contribution to the surface deformation observed by PSInSAR.

We also calculate the storativity from the additional 8 wells (Taida, Juangjing, Banqiao, Luzou, Youth Park, Xinzhuang, Erchong and Sanchong) by the above-mentioned method (Table 1) except the Taida well, where the storativity is roughly constant across most of the aquifer with values between 0.5×10^{-4} and 1.6×10^{-3} in Jingmei Formation and 0.8×10^{-4} and 1.4×10^{-3} in Wuku Formation (Table 1). The calculated storativities are in good agreement with values from water pumping test in Jingmei Formation ranging from 1×10^{-3} to 4×10^{-3} (Chia et al., 1999). Besides, the storativity is significantly increased westward. This trend fits well with the deposit depth within the Taipei Basin (Fig. 12). Under the Jingmei formation (Fig. 2), it is worthy to note that the transient deformation induced from groundwater change is basin-wide, which should be related to the distribution of stratigraphy and its hydro-geologic condition. This preliminary result suggested that ground deformation is most likely related to the distribution of Jingmei and Wuku Formations which are the main confined aquifers in the Taipei Basin.

Based on the InSAR-derived surface deformation and groundwater wells in Tainan Tableland, Huang et al. (2016) calculate that the storativity varies from 0.0047 in 1996–2001 to 0.0075 in 2004–2009. Chaussard et al. (2014) suggested that InSAR combined with hydraulic data can characterize the aquifer-system properties at basin scale. In the future, the storativity can be converted to specific storage and values of aquifer compressibility for water resources management in Taiwan.

5. Conclusion

In this paper, we characterize the transient surface deformation in Taipei metropolitan area induced by groundwater change by using high resolution X-band time series analysis form September 2011 to July 2013. Based on 8 well data in the Taipei basin, the calculated storativity is roughly constant with values between 0.5×10^{-4} and 1.6×10^{-3} in Jingmei Formation and 0.8×10^{-4} and 1.4×10^{-3} in Wuku Formation. The transient deformation in LOS of PSInSAR suggested that the severe land subsidence in the Taipei Basin is highly related to confined aquifer deformation of Jingmei and Wuku Formations. Thus the distribution and thickness of Jingmei and Wuku Formations is an important issue for study groundwater induced deformation in the Taipei Basin. In future study, how to discriminate tectonic movement from anthropogenic or seasonal effects is a crucial issue to assess geohazards of seismogenic Shanchiao Fault. We propose a detailed investigation of ground deformation induced by groundwater change by dense continuous GPS network in the Taipei Basin and time series analysis from PSInSAR with the hydro-geological information of major confined aquifers in the Taipei Basin. For instance, with only three continuous GPS stations available in the Taipei Basin (Fig. 3), the deployment of a dense continuous GPS network should be the first concern in a study of the activity of the Shanchiao Fault.

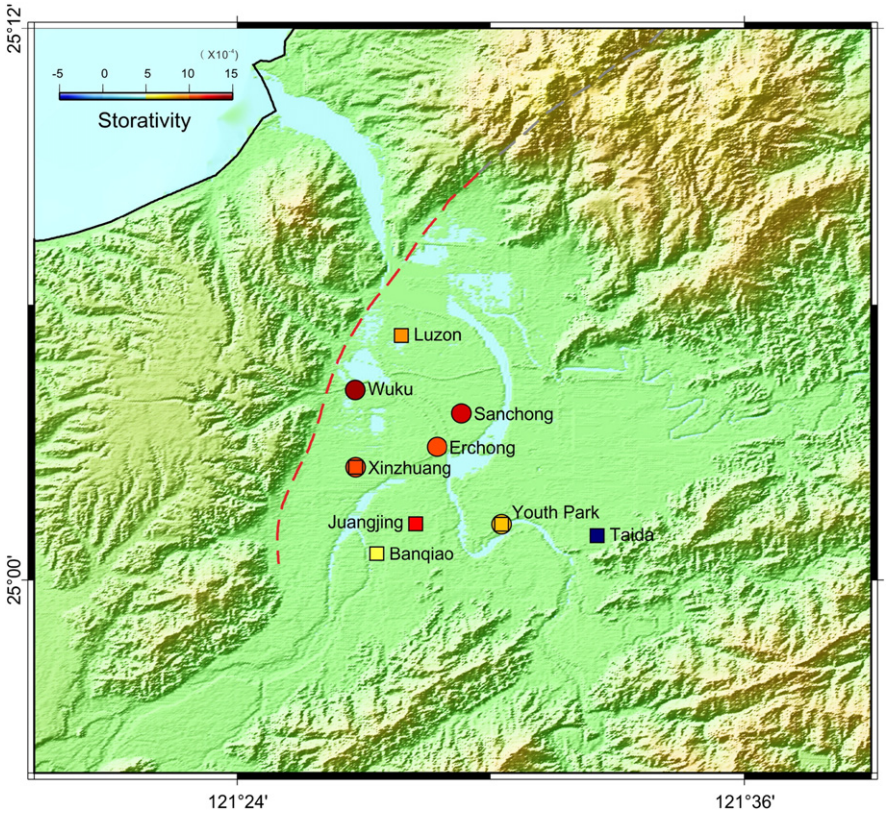

Fig. 12. Storativity calculated in 9 wells within the Taipei Basin. Square and circle represent the location of the well in Jingmei Formation and Wuku Formation, respectively. Circle with square inside represents well located both in Jingmei and Wuku Formations.

Acknowledgments

The comments and suggestions from two anonymous reviewers are deeply appreciated. This study was supported by Drunken Moon Lake Research Platform between National Taiwan University and Academia Sinica (102R3257 and 103R3253). The support is also from Ministry of Science and Technology Taiwan under the grant 102–2811-M-002-065. Leveling data is provide by Central Geological Survey, MOEA (102-5226904000-06-01, 103-5226904000-04-01 and 104-5226904000-03-01). We are grateful to Fabio Bovenga, Janusz Wasowski and Akiko Tanaka for their valuable comments and suggestions

References

Abidin, H.Z., Djaja, R., Darmawan, D., Hadi, S., Akbar, A., Rajiyowiryono, H., Sudibyo, Y., Meilano, I., Kasuma, M.A., Kahar, J., Subarya, C., 2001. Land subsidence of Jakarta (Indonesia) and its geodetic monitoring system. Nat. Hazards 23, 365–387.

Allen, D.R., Mayuga, M.N., 1969. The Mechanics of Compaction and Rebound, Wilmington Oil Field, Long Beach, California, USA, International Hydrological Decade, Symposium on Land Subsidence, Tokyo, Japan 17–22 Sept.

Amelung, F.D., Galloway, L., Bell, J.W., Zebker, H.A., Laczniak, R.J., 1999. Sensing the ups and downs of Las Vegas: InSAR reveals structural control of land subsidence and aquifer-system deformation. Geology 27 (6), 483–486. http://dx.doi.org/10.1130/0091-7613(1999)027<0483:STUADO>2.3.CO;2.

Bell, J.W., Amelung, F., Ferretti, A., Bianchi, M., Novali, F., 2008. Permanent scatterer InSAR reveals seasonal and long-term aquifer-system response to groundwater pumping and artificial recharge. Water Resour. Res. 44, W02407. http://dx.doi.org/10.1029/2007WR006152.

Berardino, P., Fornaro, G., Lanari, R., Sansosti, E., 2002. A new algorithm for surface deformation monitoring based on small baseline differential SAR interferograms. IEEE Trans. Geosci. Remote Sens. 40 (11), 2375–2383.

Buckley, S.M., Rosen, P.A., Hensley, S., Tapley, B.D., 2003. Land subsidence in Houston, Texas, measured by radar interferometry and constrained by extensometers. J. Geophys. Res. 108 (B11), 2542. http://dx.doi.org/10.1029/2002JB001848.

Bürgmann, R., Rosen, P.A., Fielding, E.J., 2000. Synthetic aperture radar interferometry to measure Earth's surface topography and its deformation. Annu. Rev. Earth Planet. Sci. 28, 169–209.

Champenois, J., Fruneau, B., Pathier, E., Deffontaines, B., Lin, K.-C., Hu, J.-C., 2012. Monitoring of active tectonic deformations in the Longitudinal Valley (eastern Taiwan) using persistent scatterer InSAR method with ALOS PALSAR data. Earth Planet. Sci. Lett. 337-338, 144–155. http://dx.doi.org/10.1016/j.epsl.2012.05.025.

Chang, C.-P., Yen, J.-Y., Hooper, A., Chou, F.-M., Chen, Y.-A., Hou, C.-S., Hung, W.-C., Lin, M.-S., 2010. Monitoring of surface deformation in northern Taiwan using DInSAR and PSInSAR techniques. Terr. Atmos. Ocean. Sci. 21 (3), 447–461. http://dx.doi.org/10.3319/TAO.2009.11.20.01(TH).

Chang, K.-J., Shyu, J.B.H., Chen, R.-F., Chan, Y.-C., Yeh, E.-C., Lai, K.-Y., 2014. Study and investigate characteristics of important active faults: Analyze and interpret near fault high resolution geomorphological data. Project Report, Central Geological Survey, MOEA, p. 327 (in Chinese with English abstract).

Chaussard, E., Amelung, F., Abidin, H., Hong, S.-H., 2013. Sinking cities in Indonesia: ALOS PALSAR detects rapid subsidence due to groundwater and gas extraction. Remote Sens. Environ. 128, 150–161. http://dx.doi.org/10.1016/j.rse.2012.10.015.

Chaussard, E., Bürgmann, R., Shirzaei, M., Fielding, E.J., Baker, B., 2014. Predictability of hydraulic head changes and characterization of aquifer-system and fault properties from InSAR-derived ground deformation. J. Geophys. Res. Solid Earth 119, 6572–6590. http://dx.doi.org/10.1002/2014JB011266.

Chen, C.-T., Lee, J.-C., Hu, J.-C., Chan, Y.-C., Lu, C.-Y., 2006. The active Shanchiao Fault in the Metropolitan Taipei area, northern Taiwan: geomorphic and geodetic analyses. Eos, Trans., AGU, 87–52, Fall Meeting Supplement, Abstract T33D-0543.

Chen, C.-T., Hu, J.-C., Lu, C.-Y., Lee, J.-C., Chan, Y.-C., 2007. Thirty-year land elevation change from subsidence to uplift following the termination of groundwater pumping and its geological implications in the Metropolitan Taipei Basin, northern Taiwan. Eng. Geol. 95, 30–47. http://dx.doi.org/10.1016/j.enggeo.2007.09.001.

Chen, C.-T., Lee, J.-C., Chan, Y.-C., Lu, C.-Y., 2010a. Growth normal faulting at the western edge of the Metropolitan Taipei Basin since the last Glacial Maximum, northern Taiwan. Terr. Atmos. Ocean. Sci. 21 (3), 447–461. http://dx.doi.org/10.3319/TAO.2009.11.20.01(TH).

Chen, C.-T., Lee, J.-C., Chen, Y.-C., Lu, C.-Y., Teng, S.-Y., 2014. Elucidating the geometry of the active Shanchiao fault in the Taipei metropolis, northern Taiwan, and the reactivation relationship with pre-existing orogen structures. Tectonics 33, 2400–2418. http://dx.doi.org/10.1002/2013TC003502.

Chen, K.-C., Huang, B.-S., Huang, W.-G., Wang, J.-H., Kim, K.-H., Lee, S.-J., Lai, Y.-C., Tsao, S., Chen, C.-H., 2010b. A blind normal fault beneath the Taipei Basin in northern Taiwan. Terr. Atmos. Ocean. Sci. 21 (3), 495–502. http://dx.doi.org/10.3319/TAO.2010.01.25.01(TH).

Chia, Y.-P., Chang, M.-H., Liu, W.-I., Lai, T.-C., 1999. Hydrogeologic characterization of Taipei Basin. Cent. Geol. Surv. Spec. Publ. 11, 393–406 (in Chinese with English abstract).

Crosetto, M., Castillo, M., Arbiol, R., 2003. Urban subsidence monitoring using radar interferometry: algorithms and validation. Photogramm. Eng. Remote Sens. 69, 775–783.

Ding, X.-L., Liu, G.-X., Li, Z.-W., Li, Z.-L., Chen, Y.-Q., 2004. Ground subsidencemonitoring in Hong Kong with satellite SAR interferometry. Photogramm. Eng. Remote Sens. 70 (10), 1151–1156.

Ferretti, A., Prati, C., Rocca, F., 2000. Nonlinear subsidence rate estimation using permanent scatterers in differential SAR interferometry. IEEE Trans. Geosci. Remote Sens. 38, 2202–2212.

Ferretti, A., Prati, C., Rocca, F., 2001. Permanent scatterers in SAR interferometry. IEEE Trans. Geosci. Remote Sens. 39 (1), 8–20.

Galloway, D.L., Hoffmann, J., 2007. The application of satellite differential SAR interferometry-derived ground displacements in hydrogeology. Hydrogeol. J. 15, 133–154.

Holzer, T.L., 1984. Ground failure induced by groundwater withdrawal from unconsolidated sediments. Rev. Eng. Geol. 6, 67–105.

Hooper, A., Zebker, H., Segall, P., Kampes, B., 2004. A new method for measuring deformation on volcanoes and other natural terrains using InSAR persistent scatterers. Geophys. Res. Lett. 31 (23), L23611. http://dx.doi.org/10.1029/2004GL021737.

Hou, C.-S., Hu, J.-C., Shen, L.-C., Wang, J.-S., Chen, C.-L., Lai, T.-C., Huang, C., Yang, Y.-R., Chen, R.-F., Chen, Y.-G., Angelier, J., 2005. Estimation of subsidence using GPS measurements, and related hazard: the Pingtung Plain, southwestern Taiwan. Compt. Rendus Geosci. 337, 1184–1193.

Hsieh, C.-S., Shih, T.-Y., Hu, J.-C., Tung, H., Huang, M.-H., Angelier, J., 2011. Using differential SAR interferometry to map land subsidence: a case study in the Pingtung Plain of SW Taiwan. Nat. Hazards 58 (3), 1331–1332. http://dx.doi.org/10.1007/s11069-011-9734-7.

Hu, J.-C., Angelier, J., Lee, J.-C., Chu, H.-T., Byrne, D., 1996. Kinematics of convergence, deformation and stress distribution in the Taiwan collision area: 2-D finite-element numerical modelling. Tectonophysics 255, 243–268.

Hu, J.-C., Yu, S.-B., Angelier, J., Chu, H.-T., 2001. Active deformation of Taiwan from GPS measurements and numerical simulations. J. Geophys. Res. 106, 2265–2280.

Hu, J.-C., Yu, S.-B., Chu, H.-T., Angelier, J., 2002. Transition tectonics of northern Taiwan induced by convergence and trench retreat, in Byrne, T.B., and Liu, C.-S., eds., geology and geophysics of an arc–continent collision, Taiwan. Geol. Soc. Am. Spec. Pap. 358, 149–162. http://dx.doi.org/10.1130/0-8137-2358-2.147.

Hu, J.-C., Chu, H.-T., Hou, C.-S., Chen, R.-F., Lai, T.-H., Nien, P.-F., 2006. The contribution to tectonic subsidence by groundwater abstraction in the Pingtung area, southwestern Taiwan as determined by GPS measurements. Quat. Int. 147, 62–69. http://dx.doi.org/10.1016/j.quaint.2005.09.007.

Huang, S.-Y., Rubin, C.M., Chen, Y.-G., Liu, H.-C., 2007. Prehistoric earthquakes along the Shanchiao Fault, Taipei Basin, northern Taiwan. J. Asian Earth Sci. 31, 265–276. http://dx.doi.org/10.1016/j.jseaes.2006.07.025.

Huang, M.-H., Bürgmann, R., Hu, J.-C., 2016. Fifteen years of surface deformation in Western Taiwan: Insight from SAR interferometry. Tectonophysics 692, 252–264.

Hung, W.-C., Hwang, C., Chang, C.-P., Yen, J.-Y., Liu, C.-H., Yang, W.-H., 2010. Monitoring severe aquifer-system compaction and land subsidence in Taiwan using multiple sensors: Yunlin, the southern Choshui River alluvial fan. Environ. Earth Sci. 59 (7), 1535–1548. http://dx.doi.org/10.1007/s12665-009-0139-9.

Hung, W.-C., Hwang, C., Chen, Y.-A., Chang, C.-P., Yen, J.-Y., Hooper, A., Yang, C.-Y., 2011. Surface deformation from persistent scatterers SAR interferometry and fusion with leveling data: a case study over the Choshui River alluvial fan, Taiwan. Remote Sens. Environ. 115, 957–967.

Hwang, C., Hung, W.-C., Liu, C.-H., 2008. Results of geodetic and geotechnical monitoring of subsidence for Taiwan high speed rail operation. Nat. Hazards 47, 1–16. http://dx.doi.org/10.1007/s11069-007-92115.

Kampes, B.M., Hanssen, R.F., 2004. Ambiguity resolution for permanent scatterer interferometry. IEEE Trans. Geosci. Remote Sens. 42 (11), 2446–2453.

Kampes, B.M., Usai, S., 1999. Doris: the Delft Object-oriented Radar Interferometric Software. Proceedings of the 2nd International Symposium on Operationalization of Remote Sensing, Enschede, The Netherlands.

Kao, H., Shen, S.J., Ma, K.-F., 1998. Transition from oblique subduction to collision: earthquakes in the southernmost Ryukyu arc-Taiwan region. J. Geophys. Res. 103, 7211–7229.

Kim, K.-H., Chang, C.-H., Ma, K.-F., Chiu, J.-M., Chen, K.-C., 2005. Modern seismic observations in the Tatun volcano region of northern Taiwan: seismic/volcanic hazard adjacent to the Taipei metropolitan area. Terr. Atmos. Ocean. Sci. 16, 579–594.

Konikow, L.F., Kendy, E., 2005. Groundwater depletion: a global problem. Hydrogeol. J. 13, 317–320. http://dx.doi.org/10.1007/s10040-004-0411-8.

Konstantinou, K.I., Lin, C.-H., Liang, W.-T., 2007. Seismicity characteristics of a potentially active Quaternary volcano: the Tatun Volcano group, northern Taiwan. J. Volcanol. Geotherm. Res. 160, 300–318. http://dx.doi.org/10.1016/j.jvolgeores.2006.09.009.

Lai, J.-S., Chiu, C.-Y., Chang, S.-K., Hu, J.-C., Tan, Y.-C., 2010. Potential inundation hazards in the Taipei Basin induced by reactivation of the Shanchiao fault in the northern Taiwan. Terr. Atmos. Ocean. Sci. 21, 529–542. http://dx.doi.org/10.3319/TAO.2010.02.22.01(TH).

Lee, C.-T., Wang, Y., 1988. Quaternary stress changes in northern Taiwan and their tectonic implication. Proc. Geol. Soc. China 31 (1), 154–168.

Lin, C.-H., 2005. Seismicity increase after the construction of the world's tallest building: an active blind fault beneath the Taipei 101. Geophys. Res. Lett. 32, L22313. http://dx.doi.org/10.1029/2005GL024223.

Lin, C.-W., Chang, H.-C., Lu, S.-T., Shih, T.-S., and Huang, W.-J., 2000. An Introduction to the Active Faults of Taiwan: Explanatory Text for the Active Fault Map of Taiwan, Scale 1: 500,000, Second Ed. Cen. Geol. Surv. Spec. Publ., 13, 122 pp. (in Chinese with English abstract)

Lin, K.-C., Hu, J.-C., Ching, K.-E., Angelier, J., Rau, R.-J., Yu, S.-B., Tsai, C.-H., Shin, T.-C., Huang, M.-H., 2010. GPS crustal deformation, strain rate and seismic activity after the 1999 Chi-Chi earthquake in Taiwan. J. Geophys. Res. 115, B07404. http://dx.doi.org/10.1029/2009JB006417.

Liu, G.-X., Luo, X.-J., Chen, Q., Huang, D.-F., Ding, X.-L., 2008. Detecting land subsidence in Shanghai by PS-networking SAR interferometry. Sensors 8, 4725–4741.
Lu, Z., Danskin, W., 2001. InSAR analysis of natural recharge to define structure of a ground-water basin, San Bernardino, California. Geophys. Res. Lett. 28 (13), 2661–2664. http://dx.doi.org/10.1029/2000GL012753.
Lu, C.-Y., Angelier, J., Chu, H.-T., Lee, J.-C., 1995. Contractional, transcurrent, rotational and extensional tectonics: examples from northern Taiwan. Tectonophysics 246, 129–146.
Massonnet, D., Feigl, K.L., 1998. Radar interferometry and its application to changes in the Earth's surface. Rev. Geophys. 36 (4), 441–500. http://dx.doi.org/10.1029/97RG03139.
Massonnet, D., Rossi, M., Carmona, C., Adragna, F., Peltzer, G., Feigl, K., Rabaute, T., 1993. The displacement field of the Landers earthquake mapped by radar interferometry. Nature 364, 138–142.
Mora, O., Mallorqui, J.J., Broquetas, A., 2003. Linear and nonlinear terrain deformation maps from a reduced set of interferometric SAR images. IEEE Trans. Geosci. Remote Sens. 41 (10), 2243–2253.
Peyret, M., Dominguez, S., Cattin, R., Champenois, J., Leroy, M., Zajac, A., 2011. Present-day interseismic surface deformation along the Longitudinal Valley, eastern Taiwan, from a PS-InSAR analysis of the ERS satellite archives. J. Geophys. Res. 116, B03402. http://dx.doi.org/10.1029/2010JB007898.
Phien-wej, N., Giao, P.H., Nutalaya, P., 2006. Land subsidence in Bangkok, Thailand. Eng. Geol. 82, 187–201. http://dx.doi.org/10.1016/j.enggeo.2005.10.004.
Pritchard, M.E., Simons, M., 2002. A satellite geodetic survey of large-scale deformation of volcanic centres in the central Andes. Nature 418, 167–171.
Rau, R.-J., Ching, K.-E., Hu, J.-C., Lee, J.-C., 2008. Crustal deformation and block kinematics in transition from collision to subduction: GPS measurements in northern Taiwan, 1995–2005. J. Geophys. Res. 113, B09404. http://dx.doi.org/10.1029/2007JB005414.
Schmidt, D.A., Bürgmann, R., 2003. Time-dependent land uplift and subsidence in the Santa Clara valley, California, from a large interferometric synthetic aperture radar data set. J. Geophys. Res. 108 (B9), 2416. http://dx.doi.org/10.1029/2002JB002267.
Shyu, J.B.H., Sieh, K., Chen, Y.-G., Liu, C.-S., 2005. Neotectonic architecture of Taiwan and its implications for future large earthquakes. J. Geophys. Res. 110, B08402. http://dx.doi.org/10.1029/2004JB003251.
Song, S.-R., Tsao, S., Lo, H.-J., 2000. Characteristics of the Tatun volcanic eruptions, North Taiwan; implications for a cauldron formation and volcanic evolution. J. Geol. Soc. China 43, 361–378.
Suppe, J., 1981. Mechanics of mountain building and metamorphism in Taiwan. Mem. Geol. Soc. China 4, 67–89.
Teatini, P., Ferronato, M., Gambolati, G., Bertoni, W., Gonella, M., 2005. A century of land subsidence in Ravenna, Italy. Environ. Geol. 47, 831–846.
Teng, L.S., 1990. Late Cenozoic arc–continent collision in Taiwan. Tectonophysics 183, 57–76.
Teng, L.S., Yuan, P.B., Chen, P.-Y., Peng, C.-H., Lai, T.-C., Fei, L.-Y., Liu, H.-C., 1999. Lithostratigraphy of Taipei Basin deposits. Cent. Geol. Surv. Spec. Publ. 11, 41–66 (in Chinese with English abstract).
Teng, L.S., Lee, C.-T., Tsai, Y.-B., Hsiao, L.-Y., 2000. Slab breakoff as a mechanism for flipping of subduction polarity in Taiwan. Geology 28, 155–158.
Teng, L.S., Lee, C.-T., Peng, C.-H., Chen, W.-F., Chu, C.-J., 2001. Origin and geological evolution of the Taipei Basin, northern Taiwan. West. Pac. Earth Sci. 1 (2), 115–142.
Tung, H., Hu, J.-C., 2012. Assessments of serious anthropogenic land subsidence in Yunlin County of Central Taiwan from 1996 to 1999 by persistent scatterers InSAR. Tectonophysics 578, 126–135. http://dx.doi.org/10.1016/j.tecto.2012.08.009.
Waltham, T., 2002. Sinking cities—Feature. Geol. Today 18 (3), 95–100.
Wang, C.-Y., Hsiao, W.-C., Sun, C.-T., 1994. Reflection seismic stratigraphy in Taipei basin (I) — northwestern Taipei basin. J. Geol. Soc. China 37, 69–95.
Wang, C.-Y., Tsai, Y.-L., Ger, M.-L., 1995. Reflection seismic stratigraphy in Taipei basin (II) — southwestern Taipei basin. J. Geol. Soc. China 38, 141–172.
Wang, J.-H., Huang, M.-W., Huang, W.-G., 2006. Aspects of M ≥ 4 earthquakes in the Taipei metropolitan area. West. Pac. Earth Sci. 6, 169–190.
Wang, C.-T., Chen, K.-S., Hu, J.-C., Chang, W.-Y., Boerner, W.M., 2011. Mapping land uplift and subsidence in the industrial parks in northern Taiwan by radar interferometry. Int. J. Remote Sens. 32 (21), 6527–6538. http://dx.doi.org/10.1080/01431161.2010.512932.
Wei, K., Chen, Y.-G., Liu, T.-K., 1998. Sedimentary history of the Taipei Basin with constraints from thermoluminescence dates. J. Geol. Soc. China 41, 109–125.
Wilson, A.M., Gorelick, S., 1996. The effects of pulsed pumping on land subsidence in the Santa Clara Valley, California. J. Hydrol. 174 (3), 375–396.
Wright, T.J., 2002. Remote monitoring of the earthquake cycle using satellite radar interferometry. Philos. Trans. R. Soc. Lond. Ser. A 360, 2873–2888. http://dx.doi.org/10.1098/rsta.2002.1094.
Wu, C.-M., 1987. Reviews on the land subsidence of the Taipei Basin (in Chinese). Sino-Geotechnics 20, 34–49.
Wu, Y.-Y., Hu, J.-C., Lin, G.-P., Chang, C.-P., Tung, H., Lu, C.-H., 2013. Transient active deformation in Tainan tableland using persistent scatterers SAR interferometry. Bull. Soc. Geol. Fr. 184 (4–5), 441–450.
Yu, S.-B., Chen, H.-Y., Kuo, L.-C., 1997. Velocity field of GPS stations in the Taiwan area. Tectonophysics 274, 41–59.
Yu, S.-B., Chen, H.-Y., Kou, L.-C., Hou, C.-S., Lee, C.-F., 1999. A study on the fault activities of the Taipei Basin. Spec. Publ. Cent. Geol. Surv. 11, 227–251 (in Chinese with English abstract).